tion of each sample was measured by the method of Bradford (Bio-Rad, Hercules, CA, U.S.A.).[24] Electrophoresis was performed with samples containing 50 μg of cell lysates in SDS-polyacrylamide gel electrophoresis (PAGE) loading buffer using 10% polyacrilamide gel, followed by transfer of the proteins onto pure nitrocellulose membranes (Trans-Blot Transfer Membrane; Bio-Rad). Immunoreactivity was detected by enhanced chemiluminescence (Amersham Biosciences). The relative density of bands was determined by Intelligent Quantifier program (Bio Image, Ann Arbor, MI, U.S.A.) and normalized to the loading control.

RESULTS

ρ^0 Cells Lacking mtDNA

ρ^0 cells lacking mtDNA (named HeLa EB8-C) were made by long-term EtBr treatment.[23] ρ^+ cells (HeEB5) were cybrids of EB8-C cells with intact mtDNA. To confirm the absence of mtDNA, the 298-bp segment of mtDNA was amplified by polymerase chain reaction (PCR) analysis (Fig. 1). No detectable band corresponding to mtDNA was noted in EB8-C cells, whereas clear bands were amplified in HeEB5 cells. We also confirmed the absence of mtDNA by the failure to grow in the absence of uridine in the medium, since ρ^0 cells are dependent on uridine and pyruvate for growth because of the absence of a functional respiratory chain[22] (data not shown). Thus, EB8-C cells were proven to be defective in oxidative phosphorylation and were used in the present study.

Lower Production of ROS in EB8-C Cells

CM-H_2DCFDA was used for experiments because of its better retention within cells than DCF. We compared ROS generation in HeEB5 and EB8-C cells by flow cytometry. The mean fluorescence intensities of untreated HeEB5 and EB8-C cells were 51 ± 4 and 26 ± 2, respectively, indicating that HeEB5 cells produced ROS constitutively at a higher level than EB8-C cells ($p < 0.005$).

The ROS production is known to increase after irradiation in cells.[12,25] The generation of ROS was evaluated at 30 min after irradiation in the two cell lines. Exposure to irradiation with 20 Gy resulted in significantly increased fluorescence intensity in HeEB5 cells (136 ± 10, 2.6-fold, $p < 0.01$), but the fluorescent intensities were not increased in EB8-C cells (23 ± 1).

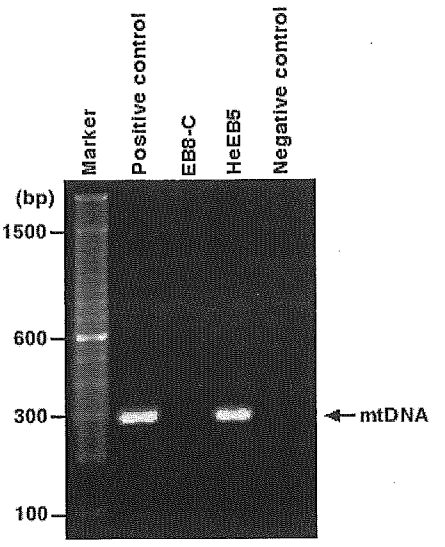

Fig. 1. Comparison between EB8-C and HeEB5 Cells
mtDNA was amplified by PCR as described in MATERIALS AND METHODS. The arrow indicates 298-bp fragments of mtDNA. SK-HEP-1 hepatocellular carcinoma cells were used as positive control. As negative control, purified water was used.

The specificity of ROS was also determined by irradiation in the presence of catalase from human erythrocytes (Calbiochem, La Jolla, CA, U.S.A.) in HeEB5 cells. The treatment with catalase abolished the irradiation-induced increase in the fluorescent intensity (data not shown). Furthermore, irradiated HeEB5 cells were stained with dihydroethidium (DHE, Molecular Probes) specific for superoxide radicals. However, an increased intensity of fluorescence was not detected in these cells (data not shown). These results suggest that irradiation increased the level of ROS, mainly hydrogen peroxide in HeEB5 cells.

Increased Sensitivity of EB8-C Cells to Irradiation

Next we sought to determine whether the observed difference in ROS production affects the survival and growth of cells after irradiation. Cellular radiosensitivity was analyzed by colony formation assay. The plating efficiencies were 87.7 ± 2.5 and 50.3 ± 4.5% in HeEB5 cells and EB8-C cells, respectively, and the efficiency was significantly reduced in EB8-C cells ($p < 0.001$). Further study found a significantly reduced survival fraction in EB8-C irradiated with 2 Gy (Fig. 2). The surviving fractions were 0.33 ± 0.01 and 0.19 ± 0.03 in HeEB cells and EB8-C cells, respectively ($p < 0.01$). At 4 Gy of irradiation, the fractions were 0.21 ± 0.02 for HeEB5 cells and 0.06 ± 0.00 for EB8-C cells,

showing a significantly decreased survival fraction in EB8-C cells compared to HeEB5 cells ($p < 0.005$). Upon irradiation with either 6 or 8 Gy, significant differences in sensitivity to irradiation were observed between these cell lines.

To further evaluate the cell growth after irradiation, the diameter of the colonies was quantitatively evaluated (Table 1). HeEB5 cells had a significantly higher capacity for forming colonies larger than 1.2 mm in diameter than EB8-C cells. The capacity for forming larger colonies was 15.1 ± 1.7% in the control. On the other hand, 5.5 ± 0.2% of untreated EB8-C cells formed larger colonies. HeEB5 cells also formed larger colonies than EB8-C cells at each dose of irradiation. At 1 Gy, HeEB5 cells had 14.7 ± 3.1% of the capacity, whereas that of EB8-C cells was 1.8 ± 0.4%. Thus, depleting mtDNA affected cell growth and resulted in an increased sensitivity to irradiation.

Dysfunction of the G2 Checkpoint in Irradiated EB8-C Cells

Cells have mechanisms to delay or halt cell cycle progression in response to genotoxic insult to maintain genomic integrity.[26] HeLa cells are known to be infected with human papilloma virus, of which the E6 protein inactivates p53; the checkpoint may not function in cells exposed to ionizing radiation.[27] To determine whether such checkpoint mechanisms are associated with the observed sensitivity to irradiation in EB8-C cells, cell cycle progression after irradiation was studied (Table 2). Without irradiation, the cell cycle profiles of both cell lines were similar. After irradiation with 8 Gy, 60% of HeEB5 cells had entered the G2 phase by 12 hr. Thereafter, the cells gradually re-entered G1 and then S phase by 36 hr. On the other hand, the cell cycle progression was delayed after irradiation in EB8-C cells when compared to HeEB5 cells. Cells gradually entered the G2 phase by 24 hr, and 60% of cells remained at G2 phase 36 hr after irradiation. Thus, EB8-C cells showed delayed induction of G2 arrest and decreased ability to recover from G2 arrest.

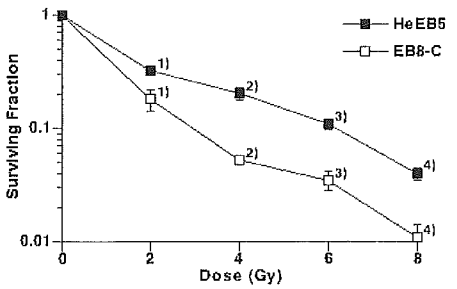

Fig. 2. Radiosensitivity of Cells Lacking mtDNA

HeEB5 and EB8-C cells were exposed to ionizing radiation at indicated doses. After two weeks, colonies were stained with hematoxilin-eosin and counted. All experiments were triplicated. The results were the mean of three independent experiments. 1) $p < 0.01$, 2–4) $p < 0.005$.

Activation of ERK Pathway in Irradiated HeEB5 Cells

Previously, we have shown that MAPK is involved in the sensitivity to irradiation.[28] To study the mechanism causing the different sensitivity to irradiation in the two cell lines, the MAPK pathway was determined. Cells were irradiated at a dose of 8 Gy and cultured for 1 hr. Western blot analysis using antibody recognizing the phosphorylated form of ERK1/2 showed that it was more abundant in untreated HeEB5 cells than in untreated EB8-C cells; EB8-C cells had a faint band of phosphorylated form of ERK1/2 (Fig. 3). HeEB5 cells had almost 4-fold higher level of phosphorylated form of ERK1/2 as compared to that of EB8-C cells. Irradiation activated ERK1/2 by 2-fold in HeEB5 cells. However, irradiation failed to increase the level of phosphorylated form of ERK1/2 in EB8-C cells. Thus, the activation of the ERK pathway was much more prominent in HeEB5 cells than in EB8-C cells. We also studied the effect of irradiation on the phosphorylation of p38MAPK in these cells. However, phosphorylation of p38MAPK was not induced in both cell lines (data not shown).

Table 1. Numbers of Colonies Larger than 1.2 mm after Irradiation in HeEB5 and EB8-C Cells

	Percentage of larger colonies					
	0	1	2	4	6	8 (Gy)
HeEB5	15.1 ± 1.7[a)]	14.7 ± 3.1[b)]	11.9 ± 1.1[c)]	8.2 ± 1.2[d)]	6.4 ± 0.5[e)]	5.8 ± 0.9[f)]
EB8-C	5.5 ± 0.2[a)]	1.8 ± 0.4[b)]	1.4 ± 0.4[c)]	1.1 ± 0.0[d)]	0.2 ± 0.1[e)]	2.0 ± 0.2[f)]

Cells were irradiated at indicated doses and the numbers of colonies (> 1.2 mm in diameter) were calculated as described in "MATERIALS AND METHODS." All experiments were triplicated and representative results of three independent experiments are shown as mean ± S.D. *a)* $p < 0.01$, *b,d,f)* $p < 0.05$, *c,e)* $p < 0.005$.

Table 2. Cell Cycle Profile after Irradiation in HeEB5 and EB8-C Cells

		Distribution of Cells in Each Stage (%)				
	Stage	0 hr	8 hr	12 hr	24 hr	36 hr
HeEB5						
Untreated	G_1	46	51	52	54	54
	S	35	30	32	30	31
	G_2/M	19	19	16	16	15
IR (8 Gy)	G_1		19	6	48	42
	S		46	34	9	36
	G_2/M		35	60	42	22
EB8-C						
Untreated	G_1	55	57	55	55	59
	S	31	38	30	31	30
	G_2/M	14	15	15	14	11
IR (8 Gy)	G_1		31	19	3	35
	S		50	49	9	5
	G_2/M		19	32	88	60

HeEB5 and EB8-C cells were irradiated at a dose of 8 Gy and harvested at the times indicated. Cells were fixed with 70% ethanol and treated with RNase A. Then, cells were stained with propidium iodide (PI) and the DNA content was analyzed by flow cytometry using CellQuest and Modifit programs.

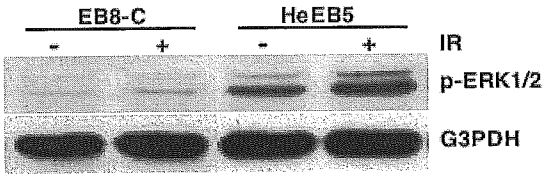

Fig. 3. Expression of ERK in Cells Exposed to Ionizing Radiation

Cells were incubated for an hour after irradiation with 8 Gy. Whole cell lysates were used for immunoblotting with anti-phosphorylated ERK1/2 antibody (Thr202/Tyr204, Cell Signaling Technology, Inc. Beverly, MA, U.S.A.). As loading control, glyceroaldehyde-3-phosphate dehydrogenase (G3PDH) was used. The results are representative of three independent experiments.

Inhibition of ERK Pathway Results in Dysfunctional G2 Checkpoint in Irradiated Cells

MEK2 activation has been reported to be essential for cellular recovery from the G2 phase arrest and subsequent survival in irradiated HeLa cells.[20] To study whether the ERK pathway is involved in the cell cycle delay of irradiated cells, cells were pretreated with MEK1/2 inhibitors, either PD98059 (50 μM) or U0126 (10 μM), for 1 hr and then irradiated at 8 Gy in the presence of these inhibitors. Twenty-four hours after irradiation, the cell cycle distribution of the cells was analyzed (Table 3). HeEB5 cells cycled more rapidly after irradiation than EB8-C cells; 62% of cells had re-entered the G1 phase by 24 hr, whereas 83% of EB8-C cells remained at the G2 phase (see also Table 2). On the other hand, treatment with either PD98059 or U0126 induced delayed recovery from the G2 checkpoint in irradiated HeEB5 cells; 46 and 57% of cells treated with PD98059 and U0126 stayed at the G2 phase 24 hr after irradiation, respectively. In contrast, treatment with either of these inhibitors did not affect the cell cycle profile in irradiated EB8-C cells.

To further determine whether ROS generated in cells exposed to irradiation affect cell cycle progression, these cells were treated with 25 mM of a free radical scavenger N-acetyl cystein (NAC) for 1 hr, and then irradiated at 8 Gy in the presence of NAC. The cell cycle was analyzed 24 hr after irradiation. NAC treatment also resulted in the delayed recovery from irradiation-induced G2 arrest in HeEB5 cells; 62% of the cells were at G2/M phase. However, NAC accelerated the recovery slightly in irradiated EB8-C cells. In parallel, the numbers of colonies were counted 2 weeks later. A significantly decreased sensitivity was observed in EB8-C cells; the surviving fractions were 3.3 ± 0.8% for HeEB5 cells and 1.6 ± 0.5% for EB8-C cells, respectively ($p < 0.05$). Treatment with NAC reduced the surviving fraction in irradiated HeEB5 cells (0.7 ± 0.2%, $p < 0.05$). In contrast, pretreatment with the compound had no significant effect on the fraction of irradiated EB8-C cells (0.6 ± 0.5%).

Table 3. Effect of MEK1/2 Inhibition and ROS Scavenger on Cell Cycle Progression after Irradiation

		Distribution of Cells in Each Stage (%)				
		Untreated	IR	PD+IR	U+IR	NAC+IR
HeEB5	G_1	55	62	46	37	32
	S	30	15	8	6	6
	G_2/M	15	23	46	57	62
EB8-C	G_1	56	7	4	7	9
	S	31	10	14	12	22
	G_2/M	13	83	82	81	69

Cells were pretreated with either MEK inhibitor PD98059 (PD, 50 μM, Calbiochem, La Jolla, CA, U.S.A.), U0126 (U, 10 μM, Cell Signaling Technology, Inc., Beverly, MA, U.S.A.) or a free radical scavenger N-acetyl cysteine (NAC, 25 mM, Sigma) for 1 hr. Then cells were irradiated with 8 Gy. Twenty-four hr after irradiation, cell cycle analysis with propidium iodide staining was performed. Data are representative of three independent experiments.

DISCUSSION

ROS are ubiquitously generated at a steady state, and their production is enhanced by irradiation.[29] mtDNA is more vulnerable to oxidative stress than nuclear DNA.[2] Furthermore, mtDNA is continuously replicated even in terminally differentiated cells. It is therefore of major importance that the role(s) of mtDNA in irradiated cells is clarified. In the present study, we compared cells without mtDNA (ρ^0 cells, EB8-C) to control cells with intact mtDNA (ρ^+ cells, HeEB5) in irradiation. EB8-C cells produced less amounts of ROS than HeEB5 cells both at a steady state and following irradiation. We also showed that EB8-C cells were more sensitive to irradiation than HeEB5 cells, a phenomenon associated with lower post-irradiation ROS production. Irradiated HeEB5 cells exhibited earlier recovery from irradiation-induced G2 arrest, which was blocked by either MEK inhibition or scavenging ROS.

Induction of cell cycle checkpoint responses in cells exposed to irradiation is essential for maintaining genomic integrity by the repair of damaged DNA.[26] Oxidative stress such as irradiation causes G1 arrest that is dependent on p53 activation.[26] Since effective G2 arrest and recovery from G2 arrest have also been shown to be essential for the ability of the cell to respond effectively to irradiation, we analyzed the cell cycle profile of HeEB5 and EB8-C cells after irradiation. Following irradiation, HeEB5 cells did not arrest in the G1 phase, entering into the G2 phase. These results were consistent with a previous study reporting that the G2 checkpoint showed arrest due to irradiation damage in HeLa cells.[30] On the other hand, the cell cycle progression of irradiated EB8-C cells was delayed, as these cells induced delayed G2 arrest. In addition, HeEB5 cells exited faster from the G2 phase than EB8-C cells, with the latter demonstrating a delayed recovery from the G2 arrest. Previous studies showed that reconstitution of p53-null cells with functional p53 shortened G2 arrest upon irradiation,[31] and that bone marrow cells enriched in normal myeloblasts entered mitosis more frequently than p53-null cells after exposure to irradiation.[32,33] Moreover, in ataxia telangiectasia (AT) cells, the DNA damage-dependent G2 arrest is longer than in normal cells,[34] and the length of G2 arrest has been reported to correlate with the radioresistance of the cell.[33] These studies suggest that the prolonged G2 phase following DNA damage is due to lower repair efficiency. However, mtDNA does not code for any DNA repair protein. Therefore, our results suggest that activation of mtDNA might lead to initiating a certain signal transduction pathway that protects cells from irradiation. HeEB5 and EB8-C cells originate from HeLa cells.[23] HeLa cells are infected with human papilloma virus and the E6 protein inactivates p53.[27] $p21^{WAF1}$ is one of the cyclin dependent kinase (Cdk) inhibitors regulated by p53 and causes cell cycle arrest.[35] However, $p21^{WAF1}$ is also induced by p53-independednt mechanisms following irradiation.[36] Therefore, we studied the expression of $p21^{WAF1}$ in these cells. The $p21^{WAF1}$ expression was not induced by irradiation in HeEB5 and EB8-C cells (data not shown). Our results thus suggest that the increased sensitivity to irradiation and the delayed G2 arrest and delayed recovery from G2 arrest constitute a p53-independent event in these cells.

The MAPK pathways control cell fate in irradiated cells, and ERK signaling is important for radiation sensitivity.[16] ROS and irradiation are also known to activate MAPK pathways.[6,37,38] Moreover,

MAPK pathways are necessary for cell cycle progression through G2.[39] We studied phosphorylation of ERK1/2 in both cell lines irradiated. The phosphorylated form of ERK1/2 was clearly detected in HeEB5 cells and irradiation activated ERK1/2 in these cells. However, irradiation did not activate p38MAPK in both cells (not shown). Moreover, treatment with two different inhibitors specific for MEK1/2 delayed the recovery from G2 arrest in irradiated HeEB5 cells. Interestingly, scavenging ROS with NAC clearly induced the delayed recovery and also increased the radiation sensitivity in these cells. In EB8-C cells, however, irradiation only slightly activated the phosphorylation of ERK1/2, and NAC also induced delayed G2 arrest, albeit only to a minor extent. However, treatment with these inhibitors did not affect the cell cycle following irradiation in EB8-C cells. Thus, our study showed that the generation of ROS is involved in the regulation of the G2 checkpoint and that mtDNA is important for increased ROS generation leading to the potentiation of the ERK1/2 pathway to a certain extent in irradiated cells. It has been reported that inhibition of MEK2 upstream of ERK1/2 increased radiosensitivity through a deregulated G2 checkpoint and that treatment with caffeine reversed the radiosensitivity with a concomitant recovery from the G2 arrest in otherwise terminally arrested HeLa cells with MEK2 mutation.[20] In A431 squamous carcinoma cells and DU 145 prostate carcinoma cells, inhibition of MEK1/2 by PD 98059 slowed recovery from the G2/M arrest and enhanced cell death.[21,40] Taken together, our results indicate that the efficient activation of the ERK1/2 pathway by the generation of ROS is required for protection of cells from irradiation through the recovery from irradiation-induced G2 arrest in cells. However, mtDNA-depleted cells are unable to activate the ERK pathway because of their disability to effectively generate ROS, whereas NAPDH oxidase existing in cellular membrane and epidermal growth factor-induced production may be source of ROS outside mitochondria[10] and ROS production related to cytochrome c may be also source.[41] Thus, it is clear that mtDNA is important for signal transduction as well as oxidative phosphorylation.

mtDNA is a circular, double-stranded molecule encoding 13 proteins that compose part of complex I, III–V (ATP synthase) of the electron transport chain.[42] Mammalian mitochondria account for over 90% of cellular oxygen consumption, and 1–5% of consumed oxygen is converted to ROS in the mitochondrial respiratory chain.[43] We compared the production of ROS between EB8-C and HeEB5 cells, since the mitochondrial respiratory chain is a powerful source of ROS. HeEB5 cells had a constitutively higher level of ROS with lower activity of glutathione peroxidase (GSH-Px) than EB8-C cells (data not shown). Previous studies by other investigators have also reported decreased generation of ROS in cells lacking mtDNA.[9,10,12] We also found greater plating efficiency and larger sizes of colonies in HeEB5 cells than in EB8-C cells. These results indicate that HeEB5 cells have higher growth rate. Our results also suggest that steady-state levels of ROS produced in a regulated fashion may be required for signaling pathways controlling essential cellular function, whereas high levels of ROS may inhibit the activity of cellular components or result in damage and cell death. Thus, mtDNA may play an important role in the generation of ROS that initiate the signal transduction for cell growth.

We studied the role of mtDNA in irradiated cells and showed that EB8-C cells were more sensitive to irradiation. These results are in contrast to those of studies by other investigators, who reported that ρ^0 cells are resistant to various forms of stress such as oxidative stress, chemicals, TRAIL, and others.[6–8,44] The mechanisms responsible for these discrepancies are not clear. One of these studies concluded that up-regulation of manganese superoxide dismutase (MnSOD) and GSH-Px leads to an efficient disposal of increased oxidative stress and increased resistance against ROS in ρ^0 cells.[7] In our study, on the other hand, the activity of MnSOD was higher with no difference in that of copper-zinc superoxide dismutase (CuZnSOD) but the activity of GSH-Px was lower in HeEB5 cells, and no difference of catalase (CAT) levels were observed in both cell lines (data not shown). Increased activities of SODs lead to the accumulation of H_2O_2 unless the H_2O_2 is in turn detoxified by GSH-Px or catalase. Furthermore, our study showed that scavenging ROS with NAC significantly reduced the colony forming capacity in irradiated HeEB5 cells, whereas NAC did not affect that in irradiated EB8-C cells. We could not detect an increase of the ROS generation in cells irradiated with 8 Gy or less in our experiments. However, NAC treatment delayed the recovery from G2 in irradiated HeEB5 cells with 8 Gy and also increased the radiation sensitivity of HeEB5 cells. Our results strongly suggest that mtDNA plays an important role in initiating a certain signal transduction pathway leading to cell survival, whereas the

role of ROS may vary according to cell type and their concentrations produced.

Acknowledgements This work is supported in part by a Grant-in-Aid for Science Research from the Japan Society for the Promotion of Science (JSPS) (No. 16591242) and also a research project of the Radiation Emergency Medical Preparedness by National Institute of Radiological Sciences. We would like to thank Ms. Aki Yamamoto and Ms. Kyoko Takayama for their secretarial assistance.

REFFERENCES

1) Saraste, M. (1999) Oxidative phosphorylation at the fin de siecle. *Science*, **283**, 1488–1493.
2) Brown, W. M., George, M., Jr. and Wilson, A. C. (1979) Rapid evolution of animal mitochondrial DNA. *Proc. Natl. Acad. Sci. U.S.A.*, **76**, 1967–1971.
3) Tan, D. J., Bai, R. K. and Wong, L. J. (2002) Comprehensive scanning of somatic mitochondrial DNA mutations in breast cancer. *Cancer Res.*, **62**, 972–976.
4) Escary, J. L., Perreau, J., Dumenil, D., Ezine, S. and Brulet, P. (1993) Leukaemia inhibitory factor is necessary for maintenance of haematopoietic stem cells and thymocyte stimulation. *Nature* (London), **363**, 361–364.
5) Marchetti, P., Susin, S. A., Decaudin, D., Gamen, S., Castedo, M., Hirsch, T., Zamzami, N., Naval, J., Senik, A. and Kroemer, G. (1996) Apoptosis-associated derangement of mitochondrial function in cells lacking mitochondrial DNA. *Cancer Res.*, **56**, 2033–2038.
6) Jiang, S., Cai, J., Wallace, D. C. and Jones, D. P. (1999) Cytochrome c-mediated apoptosis in cells lacking mitochondrial DNA. Signaling pathway involving release and caspase 3 activation is conserved. *J. Biol. Chem.*, **274**, 29905–29911.
7) Park, S. Y., Chang, I., Kim, J. Y., Kang, S. W., Park, S. H., Singh, K. and Lee, M. S. (2004) Resistance of mitochondrial DNA-depleted cells against cell death: role of mitochondrial superoxide dismutase. *J. Biol. Chem.*, **279**, 7512–7520.
8) Kim, J. Y., Kim, Y. H., Chang, I., Kim, S., Pak, Y. K., Oh, B. H., Yagita, H., Jung, Y. K., Oh, Y. J. and Lee, M. S. (2002) Resistance of mitochondrial DNA-deficient cells to TRAIL: role of Bax in TRAIL-induced apoptosis. *Oncogene*, **21**, 3139–3148.
9) Li, N., Ragheb, K., Lawler, G., Sturgis, J., Rajwa, B., Melendez, J. A. and Robinson, J. P. (2003) Mitochondrial complex I inhibitor rotenone induces apoptosis through enhancing mitochondrial reactive oxygen species production. *J. Biol. Chem.*, **278**, 8516–8525.
10) Walford, G. A., Moussignac, R. L., Scribner, A. W., Loscalzo, J. and Leopold, J. A. (2003) Hypoxia potentiates nitric oxide-mediated apoptosis in Endothelial cells via peroxynitrite-induced activation of mitochondria-dependent and -independent pathways. *J. Biol. Chem.*, **279**, 4425–4432.
11) Sidoti-de Fraisse, C., Rincheval, V., Risler, Y., Mignotte, B. and Vayssiere, J. L. (1998) TNF-alpha activates at least two apoptotic signaling cascades. *Oncogene*, **17**, 1639–1651.
12) Leach, J. K., Van Tuyle, G., Lin, P. S., Schmidt-Ullrich, R. and Mikkelsen, R. B. (2001) Ionizing radiation-induced, mitochondria-dependent generation of reactive oxygen/nitrogen. *Cancer Res.*, **61**, 3894–3901.
13) Nemoto, S., Takeda, K., Yu, Z. X., Ferrans, V. J. and Finkel, T. (2000) Role for mitochondrial oxidants as regulators of cellular metabolism. *Mol. Cell. Biol.*, **20**, 7311–7318.
14) Waypa, G. B., Chandel, N. S. and Schumacker, P. T. (2001) Model for hypoxic pulmonary vasoconstriction involving mitochondrial oxygen sensing. *Circ. Res.*, **88**, 1259–1266.
15) Nishikawa, T., Edelstein, D., Du, X. L., Yamagishi, S., Matsumura, T., Kaneda, Y., Yorek, M. A., Beebe, D., Oates, P. J., Hammes, H. P., Giardino, I. and Brownlee, M. (2000) Normalizing mitochondrial superoxide production blocks three pathways of hyperglycaemic damage. *Nature* (London), **404**, 787–790.
16) Dent, P., Yacoub, A., Fisher, P. B., Hagan, M. P. and Grant, S. (2003) MAPK pathways in radiation responses. *Oncogene*, **22**, 5885–5896.
17) Shonai, T., Adachi, M., Sakata, K., Takekawa, M., Endo, T., Imai, K. and Hareyama, M. (2002) MEK/ERK pathway protects ionizing radiation-induced loss of mitochondrial membrane potential and cell death in lymphocytic leukemia cells. *Cell Death Differ.*, **9**, 963–971.
18) Tran, S. E., Holmstrom, T. H., Ahonen, M., Kahari, V. M. and Eriksson, J. E. (2001) MAPK/ERK overrides the apoptotic signaling from Fas, TNF, and TRAIL receptors. *J. Biol. Chem.*, **276**, 16484–16490.
19) Yang, S. H., Sharrocks, A. D. and Whitmarsh, A. J. (2003) Transcriptional regulation by the MAP kinase signaling cascades. *Gene*, **320**, 3–21.
20) Abbott, D. W. and Holt, J. T. (1999) Mitogen-activated protein kinase kinase 2 activation is essential for progression through the G2/M checkpoint arrest in cells exposed to ionizing radiation. *J. Biol. Chem.*, **274**, 2732–2742.

21) Hagan, M., Wang, L., Hanley, J. R., Park, J. S. and Dent, P. (2000) Ionizing radiation-induced mitogen-activated protein (MAP) kinase activation in DU145 prostate carcinoma cells: MAP kinase inhibition enhances radiation-induced cell killing and G2/M-phase arrest. *Radiat. Res.*, **153**, 371–383.
22) King, M. P. and Attardi, G. (1989) Human cells lacking mtDNA: repopulation with exogenous mitochondria by complementation. *Science*, **246**, 500–503.
23) Hayashi, J., Ohta, S., Kikuchi, A., Takemitsu, M., Goto, Y. and Nonaka, I. (1991) Introduction of disease-related mitochondrial DNA deletions into HeLa cells lacking mitochondrial DNA results in mitochondrial dysfunction. *Proc. Natl. Acad. Sci. U.S.A.*, **88**, 10614–10618.
24) Bradford, M. M. (1976) A rapid and sensitive method for the quantitation of microgram quantities of protein utilizing the principle of protein-dye binding. *Anal. Biochem.*, **72**, 248–254.
25) Morales, A., Miranda, M., Sanchez-Reyes, A., Biete, A. and Fernandez-Checa, J. C. (1998) Oxidative damage of mitochondrial and nuclear DNA induced by ionizing radiation in human hepatoblastoma cells. *Int. J. Radiat. Oncol. Biol. Phys.*, **42**, 191–203.
26) Shackelford, R. E., Kaufmann, W. K. and Paules, R. S. (2000) Oxidative stress and cell cycle checkpoint function. *Free Radic. Biol. Med.*, **28**, 1387–1404.
27) Werness, B. A., Levine, A. J. and Howley, P. M. (1990) Association of human papillomavirus types 16 and 18 E6 proteins with p53. *Science*, **248**, 76–79.
28) Takada, Y., Hachiya, M., Park, S. H., Osawa, Y., Ozawa, T. and Akashi, M. (2002) Role of reactive oxygen species in cells overexpressing manganese superoxide dismutase: mechanism for induction of radioresistance. *Mol. Cancer Res.*, **1**, 137–146.
29) Yang, Y. and Yu, X. (2003) Regulation of apoptosis: the ubiquitous way. *FASEB J.*, **17**, 790–799.
30) Maity, A., Kao, G. D., Muschel, R. J. and McKenna, W. G. (1997) Potential molecular targets for manipulating the radiation response. *Int. J. Radiat. Oncol. Biol. Phys.*, **37**, 639–653.
31) Schwartz, D., Almog, N., Peled, A., Goldfinger, N. and Rotter, V. (1997) Role of wild type p53 in the G2 phase: regulation of the gamma-irradiation-induced delay and DNA repair. *Oncogene*, **15**, 2597–2607.
32) Lavin, M. F. and Shiloh, Y. (1997) The genetic defect in ataxia-telangiectasia. *Annu. Rev. Immunol.*, **15**, 177–202.
33) Aldridge, D. R. and Radford, I. R. (1998) Explaining differences in sensitivity to killing by ionizing radiation between human lymphoid cell lines. *Cancer Res.*, **58**, 2817–2824.
34) Hawley, R. S. and Friend, S. H. (1996) Strange bedfellows in even stranger places: the role of ATM in meiotic cells, lymphocytes, tumors, and its functional links to p53. *Genes Dev.*, **10**, 2383–2388.
35) Gartel, A. L. and Tyner, A. L. (2002) The role of the cyclin-dependent kinase inhibitor p21 in apoptosis. *Mol. Cancer Ther.*, **1**, 639–649.
36) Akashi, M., Hachiya, M., Osawa, Y., Spirin, K., Suzuki, G. and Koeffler, H. P. (1995) Irradiation induces WAF1 expression through a p53-independent pathway in KG-1 cells. *J. Biol. Chem.*, **270**, 19181–19187.
37) Torres, M. (2003) Mitogen-activated protein kinase pathways in redox signaling. *Front Biosci.*, **8**, 369–391.
38) Zhang, Z., Leonard, S. S., Huang, C., Vallyathan, V., Castranova, V. and Shi, X. (2003) Role of reactive oxygen species and MAPKs in vanadate-induced G(2)/M phase arrest. *Free Radic. Biol. Med.*, **34**, 1333–1342.
39) Abrieu, A., Doree, M. and Picard, A. (1997) Mitogen-activated protein kinase activation down-regulates a mechanism that inactivates cyclin B-cdc2 kinase in G2-arrested oocytes. *Mol. Biol. Cell.*, **8**, 249–261.
40) Park, J. S., Carter, S., Reardon, D. B., Schmidt-Ullrich, R., Dent, P. and Fisher, P. B. (1999) Roles for basal and stimulated p21(Cip-1/WAF1/MDA6) expression and mitogen-activated protein kinase signaling in radiation-induced cell cycle checkpoint control in carcinoma cells. *Mol. Biol. Cell.*, **10**, 4231–4246.
41) Mikkelsen, R. B. and Wardman, P. (2003) Biological chemistry of reactive oxygen and nitrogen and radiation-induced signal transduction mechanisms. *Oncogene*, **22**, 5734–5754.
42) Anderson, S., Bankier, A. T., Barrell, B. G., de Bruijn, M. H., Coulson, A. R., Drouin, J., Eperon, I. C., Nierlich, D. P., Roe, B. A., Sanger, F., Schreier, P. H., Smith, A. J., Staden, R. and Young, I. G. (1981) Sequence and organization of the human mitochondrial genome. *Nature* (London), **290**, 457–465.
43) Boveris, A. and Chance, B. (1973) The mitochondrial generation of hydrogen peroxide. General properties and effect of hyperbaric oxygen. *Biochem. J.*, **134**, 707–716.
44) Dey, R. and Moraes, C. T. (2000) Lack of oxidative phosphorylation and low mitochondrial membrane potential decrease susceptibility to apoptosis and do not modulate the protective effect of Bcl-x(L) in osteosarcoma cells. *J. Biol. Chem.*, **275**, 7087–7094.

Instructions for Authors

The Journal of Health Science is published by the Pharmaceutical Society of Japan, and covers all aspects of health science. The Journal will publish high quality original research related to health, as effected by nutrients, endogenous factors, chemicals (including drugs), and microorganisms, employing the techniques of biochemistry, molecular biology, toxicology, and epidemiology. Reports on analytical methods and experimental techniques are also within the scope of the Journal.

The Journal will accept original and innovative submissions in English from both members and non-members of the Pharmaceutical Society of Japan, on the understanding that the work is unpublished and is not being considered for publication elsewhere.

Types of Manuscript

The Journal publishes Regular Articles, Rapid Communications, Research Letters, Reviews and Minireviews. With the exception of Reviews and Minireviews, manuscripts will be reviewed by two or more referees, whose opinions will form the basis of the final decision by the Editor.

(1) *Regular Articles*

New, significant, innovative and original findings are suitable as *Regular Articles*. Whilst the Journal does not publish Short Communications, relatively short *Regular Articles* are also acceptable if the work is of a high quality.

(2) *Rapid Communications*

These articles should be 4 or less printed journal pages. Manuscripts are reviewed rapidly. Authors are informed of the editor's decision by FAX or E-mail within 2 weeks after reception of the manuscript. The editor's decision is either acceptance or rejection for publication, and no revision process will take place. Responsibility for the scientific contents of a manuscript remains with the author. In the case of rejection, a short explanation only will be provided. When submitting *Rapid Communications*, please include a floppy disk containing the text and any figures, tables etc.

(3) *Research Letters*

Research Letters should occupy 3 printed journal pages or less. Manuscripts containing interesting findings without adequate discussion, research results of narrow scope or of a predominantly negative nature may nevertheless be suitable for publication as a *Research Letter* if they are considered sufficiently important. Subjects of relevance to health science, for example DNA sequences of unknown genes and transcriptional regulation regions etc, are also suitable as *Research Letters*. Manuscripts containing valuable data obtained in field work are also acceptable. When it is necessary to present a relatively large amount of data in field work, the paper may extend to more than 3 printed pages.

(4) *Reviews and Minireviews*

Reviews and Minireviews are submitted by invitation from the Editorial Board, and encompass recent important scientific discoveries. *Minireviews* mainly involve a description of recent research results from the author's laboratory. *Reviews* are more broad based. Whilst *Reviews* do not have a page limit, *Minireviews* should be 3 pages or less of printed Journal space.

Submission of Manuscripts

Manuscripts (in triplicate) should be submitted to :

(From Japan)
Journal of Health Science Editorial Office
The Pharmaceutical Society of Japan
2-12-15, Shibuya, Shibuya-ku, Tokyo 150-0002, Japan

(From the rest of the world)
Dr. Y. James Kang
Associate Editor, Journal of Health Science
Department of Medicine,
University of Louisville School of Medicine
511 S. Floyd St., MDR 530, Louisville, Kentucky 40202, U.S.A.

Manuscript Preparation

(1) *Manuscript Form* : All manuscripts should be typewritten in English on A4 paper, double space (24 lines per page, approx. 70 strokes per line). Since after printing, one page contains about 4300 characters, please take care when preparing the paper to not exceed the allowed length for the specific type of manuscript. The top (title) page should be numbered 1 at the bottom center. All subsequent pages should be numbered consecutively.

(2) *Title Page* : The title page (page 1) should start with the title, name(s) of the author(s) and affiliation and mailing address. An asterisk (*) should be added to the right of the corresponding author's name. Below the authors address(es) should be included the type of manuscript (Regular Article, Research Letter etc.) and the corresponding author's name, address, telephone number, fax number, and E-mail address.

(3) *Summary and Keywords* : Page 2 should contain a summary of less than 250 words and 3 to 6 descriptive key words, listed in order of importance. The first 3 key words must be independent, as they will be used in a key-word combination in the index.

(4) *Main Text* : The main text should start from page 3 and be divided into the follow sections: Introduction, Materials and Methods, Results, Discussion, Acknowledgments, and References. It is also acceptable to merge the Results

with the Discussion in the form: Results and Discussion.

(5) *Abbreviations and Units* : Abbreviation must be spelled out in full at their initial appearance, followed by the abbreviation in parentheses. Thereafter, the abbreviation may be employed. The following units should be used: length (m, cm, mm, nm, μm, Å), mass (kg, g, mg, μg, ng, pg, mol, mmol), volume (l, ml, μl), time (sec, min, hr), temperature (°C), radiation (Bq, Ci, Sv, Gy), concentration (M, mM, mol/l, mmol/l, mg/ml, μg/ml, %, %(v/v), ppm, ppb).

(6) *Figures* : In principle, figures prepared by the author will be used in the printed version of the journal. All figures should be numbered consecutively with Arabic numbers, and figure titles and legends are to be typed consecutively on a separate sheet. All figures should be prepared on A4 paper, and the authors name should be added at the top of each page.

(7) *Tables* : Tables should be typed on A4 paper and numbered consecutively with Arabic numbers. Any explanations of data or methods in the table should be directly below the table.

(8) *References* : References should be placed and numbered in the order of appearance in the text. Each number is to be positioned after the last relevant word with a right-half parenthesis mark, and all references should be collected together at the end of the text. Abbreviations for Journals should conform to Chemical Abstracts nomenclature.

Examples of References are as follow :

1) Kubo, U., Hwang, G. H. and Suzuki, H. (2000) Cloning and functional characterization of copper transporter. *J. Health Sci.*, **46**, 135–140.
2) Albert, B. and Hardin, T. D. (1998) *Metal Toxicology in Mammals*, Madison Press, New York.
3) Meister, B., Revel, T. M. and Caprio, M. N. (1999) Molecular mechanism of cell death. In *Handbook of Health Science* (Clarke, A. and Young, T. A., Eds.), Carrie Press, Tokyo, pp.135–137.

(9) *Notes* : Notes should be given in parentheses at the appropriate place in the text. Footnotes are not permitted.

Ethics

In scientific investigations involving human subjects, experiments should be performed in accordance with the ethical standards formulated in the Helsinki Declaration of 1964 (revised in 2000, cf. http://ohsr.od.nih.gov/). Similarly, animal experiments should follow the ethical standards formulated in the guidelines issued by the Science and International Affairs Bureau of the Japanese Ministry of Education, Science, Sports and Culture, No.141, 1987: "Animal Experiments in Universities etc."

Page Charges

Authors are required to pay charges, as outlined below :

(1) Page Charge : 4000 yen per printed page (not including tax). Charges may be changed without prior notice.
(2) Reprint Charges are as undermentioned table.
(3) Color Figures : Actual cost.
(4) The payment of page charge is required, but is not a condition for publication, since the decision for publication is made on the basis of scientific significance only. The publication charge may be waived upon request from authors who do not have funds. No free reprints of the article are provided.

Miscellaneous

(1) Any author who is not fully fluent in idiomatic English is urged to gain assistance with manuscript preparation from an appropriate person who can check and improve the English of their paper.
(2) Rejected manuscripts will not be returned to the author.
(3) Revised manuscripts must be returned with 2 months, otherwise they will be treated as new submissions.
(4) Except for Rapid Communications, a floppy disk containing text and figure files must be sent with the revised manuscript.
(5) The author is given an opportunity to proof the galley of an accepted manuscript. Major changes at this time are not permitted.
(6) Copyrights : The copyrights of all manuscripts published in Journal of Health Science belong to the Pharmaceutical Society of Japan. The author must submit a Copyright Transfer form to the Pharmaceutical Society of Japan.

(http://jhs.pharm.or.jp)

Reprint Charges

Number of Pages / Number of Reprints	1~2	3~4	5~6	7~8	9~10	Greater than 11
50	¥ 8000	¥ 9000	¥ 10000	¥ 11000	¥ 12000	¥ 13000
100	¥ 14400	¥ 16200	¥ 18000	¥ 19800	¥ 21600	¥ 23400
150	¥ 19200	¥ 21600	¥ 24000	¥ 26400	¥ 28800	¥ 31200
200	¥ 22400	¥ 25200	¥ 28000	¥ 30800	¥ 33600	¥ 36400
More than 250	¥ 110 each	¥ 120 each	¥ 130 each	¥ 150 each	¥ 160 each	¥ 180 each

・Postage included ; Tax extra. ・Color printing carries on extra surcharge of ¥80 per page.
・Reprints only available in multiples of 50.

Magnetic Resonance in Medical Sciences, Vol. 4, No. 1, p. 35-42, 2005

MAJOR PAPER

ADC Mapping of Benign and Malignant Breast Tumors

Reiko WOODHAMS[1]*, Keiji MATSUNAGA[1], Shinichi KAN[1], Hirofumi HATA[1], Masanori OZAKI[4], Keiichi IWABUCHI[2], Masaru KURANAMI[3], Masahiko WATANABE[3], and Kazushige HAYAKAWA[1]

[1]*Department of Radiology,* [2]*Department of Pathology,* [3]*Department of Surgery, Kitasato University School of Medicine*

[4]*Department of Medical Engineering and Technology, Kitasato University School of Allied Health Science*

1-15-1 Kitasato, Sagamihara, Kanagawa 228-8555, Japan

(Received March 10, 2005; Accepted May 18, 2005)

Purpose: The purpose of this study was to investigate the utility of diffusion-weighted imaging (DWI) and the apparent diffusion coefficient (ADC) value in differentiating benign and malignant breast lesions and evaluating the detection accuracy of the cancer extension.

Materials and Methods: We used DWI to obtain images of 191 benign and malignant lesions (24 benign, 167 malignant) before surgical excision. The ADC values of the benign and malignant lesions were compared, as were the values of noninvasive ductal carcinoma (NIDC) and invasive ductal carcinoma (IDC). We also evaluated the ADC map, which represents the distribution of ADC values, and compared it with the cancer extension.

Results: The mean ADC value of each type of lesion was as follows: malignant lesions, $1.22 \pm 0.31 \times 10^{-3}$ mm^2/s; benign lesions, $1.67 \pm 0.54 \times 10^{-3}$ mm^2/s; normal tissues, $2.09 \pm 0.27 \times 10^{-3}$ mm^2/s. The mean ADC value of the malignant lesions was statistically lower than that of the benign lesions and normal breast tissues. The ADC value of IDC was statistically lower than that of NIDC. The sensitivity of the ADC value for malignant lesions with a threshold of less than 1.6×10^{-3} mm^2/s was 95% and the specificity was 46%. A full 75% of all malignant cases exhibited a near precise distribution of low ADC values on ADC maps to describe malignant lesions. The main causes of false negative and underestimation of cancer spread were susceptibility artifact because of bleeding and tumor structure. Major histologic types of false-positive lesions were intraductal papilloma and fibrocystic diseases. Fibrocystic diseases also resulted in overestimation of cancer extension.

Conclusions: DWI has the potential in clinical appreciation to detect malignant breast tumors and support the evaluation of tumor extension. However, the benign proliferative change remains to be studied as it mimics the malignant phenomenon on the ADC map.

Keywords: ***breast cancer, breast MRI, DWI, fibrocystic disease, susceptibility artifact***

Introduction

The latest advancements in MRI (magnetic resonance imaging) technology have greatly expanded the utility of diffusion-weighted imaging (DWI) in the examination of various organs and diagnosis of various disorders.[1-4] DWI has already been applied in the important clinical use of diagnosis of brain ischemia and for differentiating brain abscess from metastatic brain tumor.[5,6] Moreover several studies have revealed the usefulness of DWI in characterizing brain lesions and tumors of the liver, pancreas, and ovary.[7-12] The greatest advantage of DWI in the diagnosis of neoplasm is that DWI reflects the biological character of the tissue. Furthermore, an enhancing material is not necessary. DWI is already achieving the stage of clinical application.

The use of DWI for breast cancer diagnosis is also recently being considered in clinical application.[3,13-15] Some authors showed lower ADC values for breast cancer compared with normal breast tissue. Y. Kuroki et al. also showed the utility of

*Corresponding author, Phone: +81-42-778-8453, E-mail: reiko99@db3.so-net.ne.jp

Table 1. Distribution of mean ADC values in histologic types of benign lesions

Benign Lesions	n	Mean ADC value (10^{-3} mm^2/s)
Fibrocystic disease	8	1.65±0.28
Intraductal papilloma	6	1.32±0.15
No evidence of malignancy	3	2.50±0.44
Phyllodes benign	3	2.00±0.45
Fibroadenoma	2	1.10±0.23
Atypical hyperplasia	1	1.7
Granuloma (after plastic surgery)	1	0.7
Total	24	

Table 2. Distribution of mean ADC values in histologic types of breast cancer

Malignant Lesions	n	Mean ADC value (10^{-3} mm^2/s)
IDC		
Solid tubular Ca	43	1.16±0.26
Papillotubular Ca	38	1.17±0.29
Scirrhous Ca	34	1.17±0.26
Lobular Ca	11	1.07±0.26
Malignant Phyllodes	3	1.67±0.59
Medullary Ca	2	1.05±0.28
Invasive micropapillary Ca	2	1.15±0.21
SCC	2	1.3
Mucinous Ca	2	1.75
Adenoid cystic Ca	1	1.0
NIDC or predominant NIDC		
DCIS	27	1.36±0.20
Intracystic papillary Ca	2	2.6±0.14
Total	167	

parallel imaging for breast DWI and displayed the significant difference between the ADC of malignant tumor and benign tumor.[15] Y. Guo et al. interpreted the correlation between cell density and ADC value and showed the inverse proportion between them.[3]

We investigate the usefulness of DWI for qualitative diagnosis of the breast and verify the sensitivity, specificity, and accuracy of DWI for breast cancer. We also evaluate the efficacy of the ADC map for assessing cancer extension.

Materials and Methods

Subjects: The subjects comprised 190 patients with a total of 191 lesions who had undergone MRI for breast examination due to tumor palpability, bloody secretion, calcification on mammography, and follow up after plastic surgery. All patients were female and aged between 14 and 88 years (mean age: 53 years). All patients underwent surgical resection and received definite pathological diagnosis.

Histological detail: Findings were 24 benign lesions, including 7 ductal hyperplasia, 1 sclerosing adenosis, 6 intraductal papilloma, 1 atypical ductal hyperplasia, 3 benign phyllodes tumor, 2 fibroadenoma, 1 granuloma, and 3 with no evidence of abnormality (Table 1). Malignant lesions totaled 167, including 43 solid-tubular carcinoma, 38 papillotubular carcinoma, 34 scirrhous carcinoma, 27 ductal carcinoma in situ (DCIS), 11 invasive lobular carcinoma, 2 malignant phyllodes tumor, and 14 others (Table 2). The mean size of the benign lesions was 34.0 mm (from 5 to 110 mm) and that of malignant lesions was 36.8 mm (from 7 to 60 mm).

MRI protocol: MRI was performed with a General Electric (GE) Signa CV/i 1.5T ver. 9.1 MRI unit equipped with a breast coil (surface coil). Prior to DWI, fast recovery fast spin echo (FRFSE) with CHESS was performed for fat saturation in the sagittal plane. After DWI was performed in the axial plane, 3 dimensional fast spoiled gradient recalled acquisition in the steady state (3DFSPGR) with Spec IR for fat saturation in the sagittal plane was performed before and after administration of gadopentetate dineglumine (0.2 mmol/kg). Subtraction images were produced with 3DFSPGR for identification of enhancement. 2DFSPGR with CHESS in the axial plane was performed after enhancement. Imaging parameters were as follows: 2DFRFSE (TR 3000, eff TE 85, 256×192, 3NEX), DWI [spin echo-single shot echo planar image (EPI) and motion probing gradient (MPG) were applied along the X, Y and Z axes (isotopic DWI) before and after the 180° pulses to obtain the images used for synthesizing isotropic images; b-values were 0 and 750 s/mm^2, TR/TE: 5000/61.8, image matrix: 128×128, field of view: 320×240 mm, slice thickness: 6 mm, spacing: 1 mm, 5NEX, acquisition time: 100 s], 3DFSPGR (TR 5.7, TE 1.2, flip angle: 20°, image matrix: 256×160, 2NEX), 2DFSPGR (TR 200, TE minimum, flip angle: 90°, image matrix: 512×192, 3NEX).

ADC value: All ADC values were calculated according to the formula: $ADC = -(1/b)\ln(S/So)$, where So and S are the signal intensities in the region of interest (ROI), obtained with different gradient factors (b values of 0, 750, and 1000

Table 3. Categorization of the four groups of correlation between low ADC value distribution on the ADC map and tumor distribution in the pathologic figures

Group	Distribution of Low ADC Values on ADC Map	n	%
G-1	Accurate distribution	129	77
G-2	Overestimation	15	9
G-3	Underestimation	11	7
G-4	False negative	12	7
Total		167	

G-1: Low ADC area similar to tumor distribution
G-2: Low ADC area greater than tumor distribution
G-3: Low ADC area smaller than tumor distribution
G-4: No decline in ADC

s/mm^2). ADC distribution was demonstrated on an ADC color map created with Advantage Workstation ver. 4.0 (GE). The ROI was placed in the target lesion and normal breast area on the ADC map with reference to subtraction images originating from 3DFSPGR and 2DFSPGR imaging after enhancement. The ROIs of the tumor lesions were smaller than the mass size excluding the normal tissue area. The size of the ROI in the area of normal breast tissue was 10 mm in diameter. Each ROI was positioned twice with a change of location and ADC values were averaged.

ADC values of benign lesions, malignant lesions, and normal breast tissues were compared, as were those of non-invasive ductal carcinoma (NIDC) and invasive ductal carcinoma (IDC). NIDC was considered to include predominant NIDC.

On the subject of malignant cases, we determined a low ADC value for malignant lesions as being less than 1.6×10^{-3} mm^2/s. We recognized the low ADC value area by a certain color on the ADC map and compared ADC maps with pathological figures to determine the accuracy of the ADC map for cancer extension. We categorized the pattern of correlation between the distribution of ADC values on the ADC map and the cancer extension in the pathological figure into 4 groups: Group 1 (G-1), where the area of low ADC values was almost the same as the tumor extension; Group 2 (G-2), where the area of low ADC values was wider and more than twice the area of tumor extension; Group 3 (G-3), where the area of low ADC values was smaller and less than one-half the area of tumor extension; and Group 4 (G-4), where no ADC reduction was observed (Table 3).

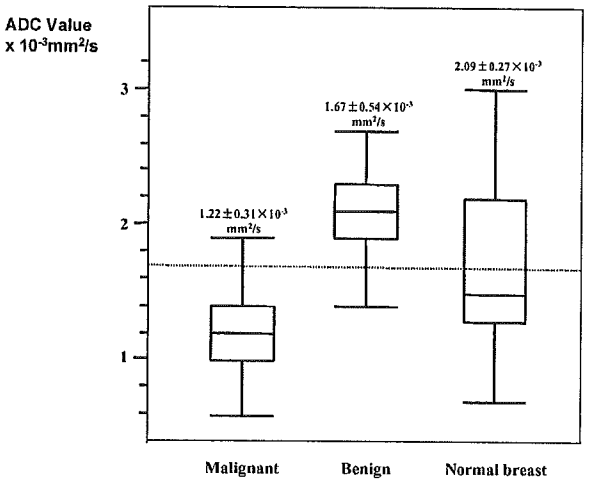

Fig. 1. Comparison among ADC values for malignant lesions, benign lesions, and normal breast tissues

Statistics

Tukey-Kramer's honesty significant difference (HSD) test was used to compare the mean ADC values of malignant tumor, benign tumor, and normal breast tissue.

The Wilcoxon signed rank sum test was used to analyze differences in the mean ADC value for significance between IDC and NIDC or predominant NIDC.

Result

Comparison of ADC values: The mean ADC value of the 167 malignant lesions was $1.22\pm0.31\times10^{-3}$ mm^2/s (ranging from 0.6 to 2.7×10^{-3} mm^2/s). The mean ADC value of the 24 benign lesions was $1.67\pm0.54\times10^{-3}$ mm^2/s (ranging from 0.7 to 3.0×10^{-3} mm^2/s), and the mean ADC value of normal breast tissue in all cases was $2.09\pm0.27\times10^{-3}$ mm^2/s (ranging from 1.4 to 3.0×10^{-3} mm^2/s). A statistically significant difference in ADC values was observed between benign tumors, malignant tumors, and normal breast tissues (Fig. 1).

The mean ADC value of IDC was $1.20\pm0.32\times10^{-3}$ mm^2/s and that of NIDC was $1.35\pm0.25\times10^{-3}$ mm^2/s. There was also significant difference ($p=0.02$) between them (Fig. 2).

Sensitivity and specificity of ADC value: With an ADC value of less than 1.6×10^{-3} mm^2/s defined as being an indicator of malignancy, 155 of the 167 malignant cases were identified as malignant lesion on the ADC map without concern for the range of ADC reduction. Sensitivity to malignant lesions was 93%. On the other hand, 13 benign cases were

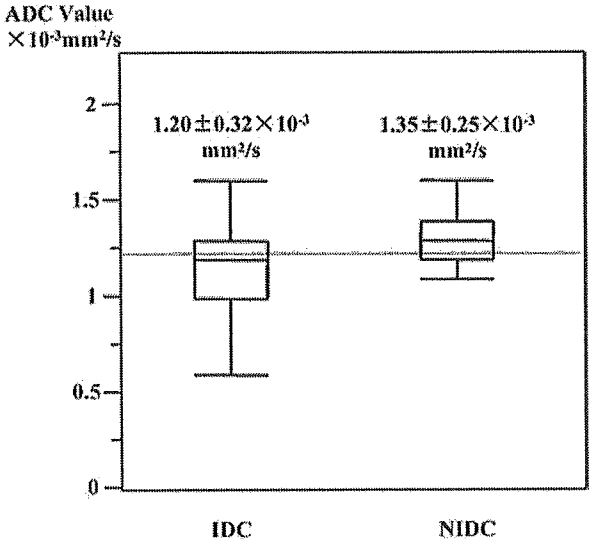

Fig. 2. Comparison between ADC values of NIDC and IDC

misdiagnosed as malignant lesions. Thus, the specificity was 46% (11/24) and the accuracy was 87% (166/191).

In 13 cases, benign lesions were misdiagnosed. The histologic details of these benign lesions were as follows: five cases of intraductal papilloma with a mean ADC value of 1.24×10^{-3} mm^2/s (ranging from 0.9 to 1.4×10^{-3} mm^2/s); three cases of fibroadenomatosis, one of ductal hyperplasia, and one of sclerosing adenosis with a mean ADC value of these lesions, fibrocystic change of 1.34×10^{-3} mm^2/s (ranging from 1.2 to 1.5×10^{-3} mm^2/s); two cases of fibroadenoma with a mean ADC value of 1.1×10^{-3} mm^2/s; and one case of granuloma with an ADC value of 0.7×10^{-3} mm^2/s.

Comparison of ADC map and histopathologic features: All malignant cases were classified into 4 groups according to the concurrence of tumor extension and distribution of low ADC values on the ADC map. A total of 129 cases were classified as G-1; 15 cases as G-2; 11 cases as G-3; and 12 cases as G-4 (Table 3).

Of the cases categorized as G-1, 11 cases represented a small compartment of DCIS foci neighboring the main tumors, which DWI did not depict. While these lesions were in the same segment as the main tumors and the sizes were less than one half as large as the main tumors, we decided to categorize such cases as G-1 (Fig. 3).

Regarding G-2, the histopathologic details of the overdiagnosed area, which showed a low ADC value of less than 1.6×10^{-3} mm^2/s instead of an absence of malignant compartment, were as follows: 1 case of apocrine metaplasia; 7 of ductal or lobular hyperplasia; 2 of blunt duct adenosis; 2 of sclerosing adenosis; 1 of fibroadenomatosis; and 2 no evidence of malignancy (Fig. 4).

With regard to G-3, the histopathologic details of the malignant component, where the ADC map did not show a low ADC value, were as follows: 4 cases showed comedo-type DCIS containing notable bleeding and necrosis, 1 case was an intracystic papillary carcinoma, 1 case showed sporadic DCIS and lobular carcinoma invasion, 2 cases were necrosis and hemorrhage section of phyllodes malignant, 2 cases were marginal zone of lobular carcinoma, and 1 case was papillotubular carcinoma. In other words, 7 cases had bleeding component in G-3. In addition, 2 cases of lobular carcinoma and 1 case of lobular carcinoma with DCIS showed sparse and small foci of tumor components in the area which the ADC map did not depict as a low ADC area (Fig. 5).

The histologic details of G-4 were as follows: 3 cases of DCIS, 2 of scirrhous carcinoma, 2 of solid tubular carcinoma, 2 of papillotubular carcinoma, and 1 each of intracystic papillary carcinoma, malignant phyllodes tumor, and mucinous carcinoma. In these cases, some notable histologic characters were seen in the specimens. Nine cases showed remarkable blood components in the specimens of malignant components (Fig. 6). In G-3 and G-4, 14 cases out of 16 with bloody components showed as high-intensity lesions in T_1-weighted images.

Discussion

According to the past reports, MRI has been confirmed as an essential tool for examination of the breasts because of its remarkably higher sensitivity with the use of enhancement material for breast carcinoma than that of ultrasound and mammography. MRI demonstrates its virtues in the research of occult cancers, where mammography and ultrasound can neither detect nor assess the cancer extension. Preoperative contrast-enhanced MRI of the breast has the potential to reveal mammographically and sonographically hidden multifocal breast carcinoma.[16-26] However, the disadvantages of MRI compared with mammography and ultrasound are the long scan times, usually 20 to 30 min, and the need for a contrast medium. In addition, the contrast material increases the cost. Furthermore, we feel that the conventional diagnostic techniques of breast MRI, morphological diagnosis and analysis of dynamic enhancement patterns, are limited to a certain degree.[27-29] On the other hand, DWI reflects some elements that affect proton diffusion, for example

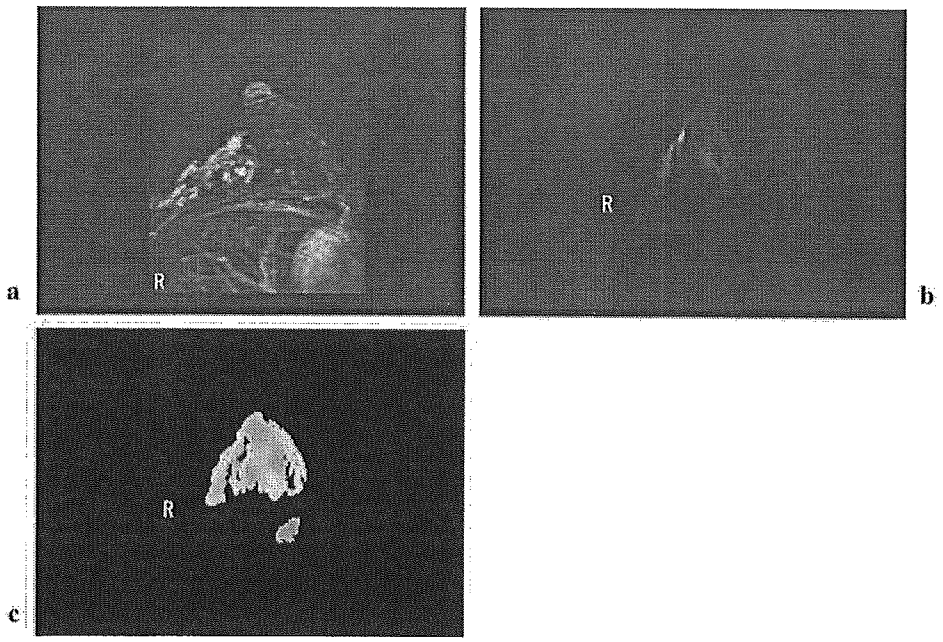

Fig. 3. A case of ductal carcinoma *in situ*
a: Maximum intensity projection (MIP) image of subtraction image obtained with 3DFSPGR. The segmental nodular enhancement is displayed in area C.
b: DWI in the axial plane shows a segmental high-intensity lesion in area C.
c: An ADC map of the same level as Fig. 3b. The greenish color indicates a low ADC value. The distribution of low ADC values corresponds to the enhancement lesion of MIP image on Fig. 3a.

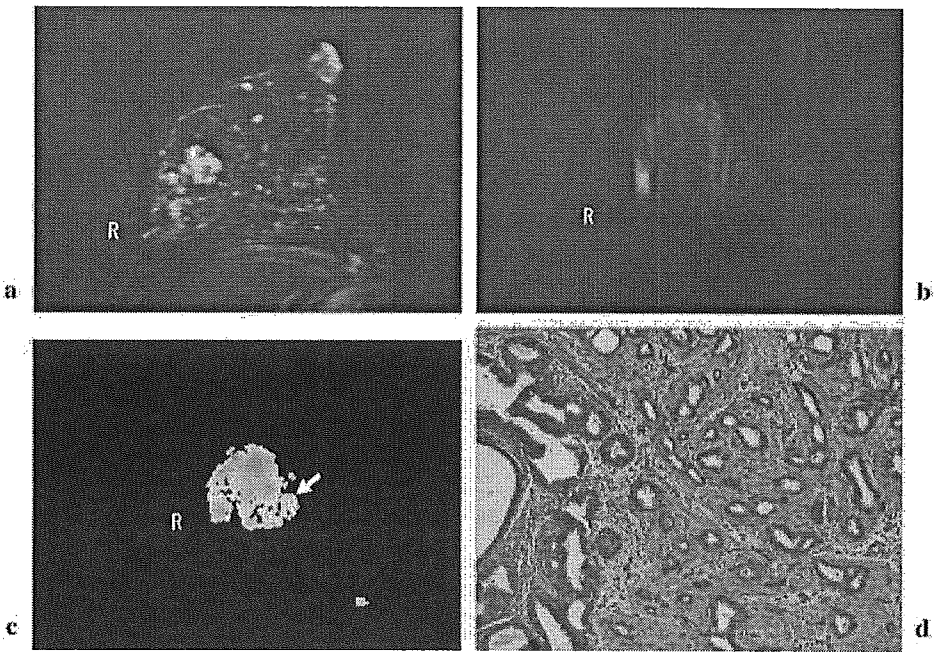

Fig. 4. A case of scirrhous carcinoma
a: MIP of subtraction image obtained with 3DFSPGR. The enhanced mass lesion in area C indicates a primary mass lesion. Note the diffuse scattering of small enhanced nodules in the mammary gland.
b: DWI reveals a high-intensity lesion in area C as a 3DFSPGR image.
c: An ADC map of the same level as Fig. 4b. The primary mass lesion shows a low ADC value. Area A also shows a low ADC region (white arrow).
d: Pathologic figure of area A. The sclerosing adenosis is prominent (H&E, ×40).

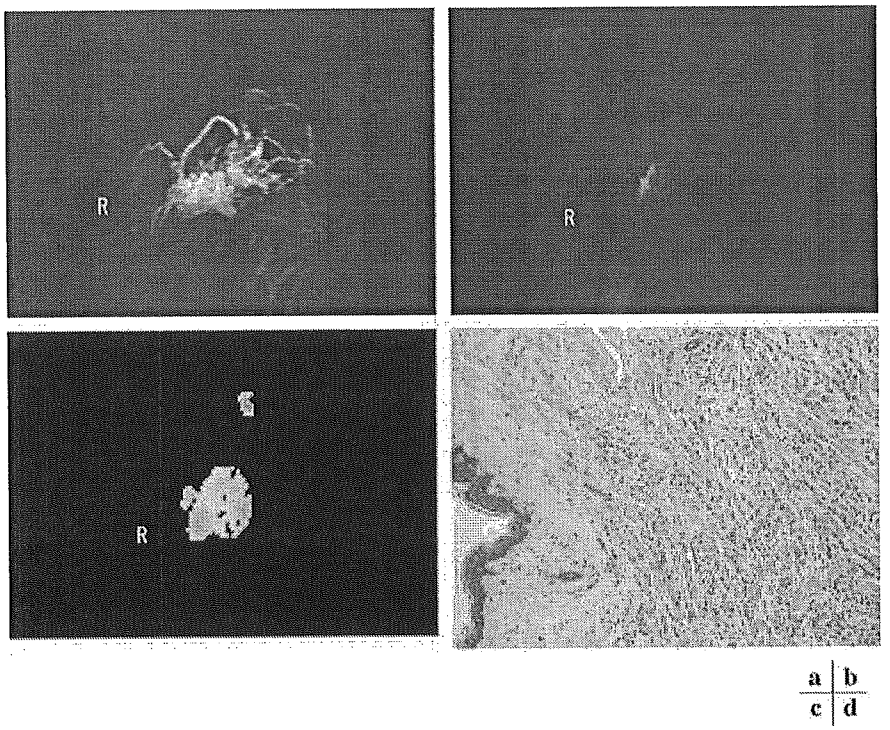

Fig. 5. A case of invasive lobular carcinoma
a: A MIP image of a subtraction image shows a speculated enhanced mass lesion extending from area A to area C. Some linear and nodular enhancements extend to the nipple site, which suggest tumor invasion.
b: DWI reveals a localized high-intensity lesion in area C that is smaller than the enhanced lesion in the 3DFSPGR image.
c: A low ADC area is evident in area C. The extending enhanced lesion obtained with 3DFSPGR is not visualized on the ADC map.
d: Histologic appearance of the area where the 3DFSPGR image shows enhancement, whereas the ADC map did not show ADC reduction (H&E, ×100). Sparse and scattered distribution of cancer cells is evident in the stroma.

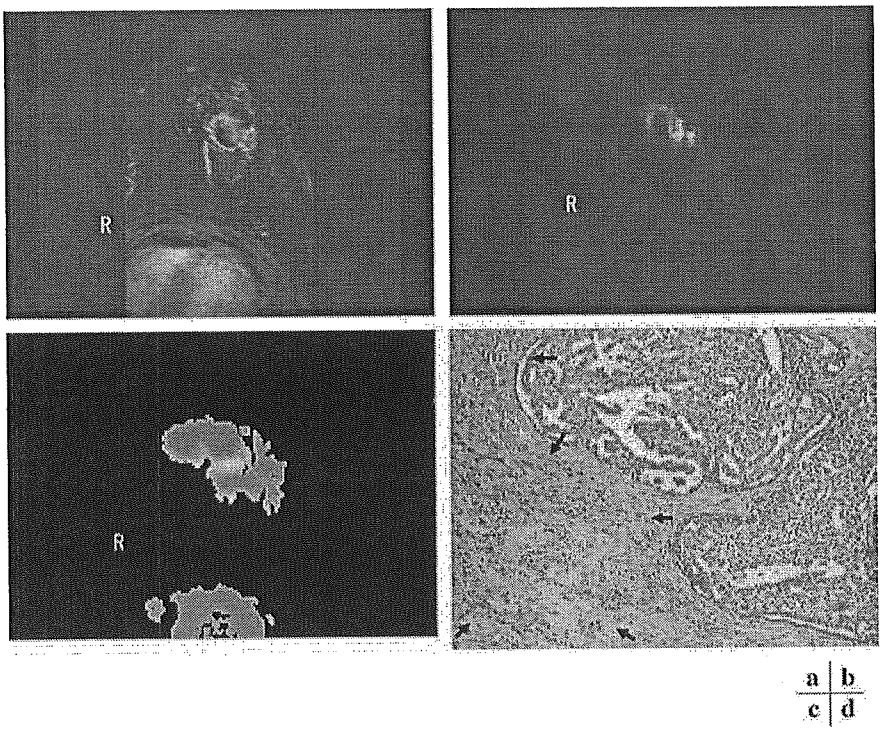

Fig. 6. A case of intracystic papillary carcinoma surrounded by intraductal carcinoma
a: A cystic mass lesion in area D. The irregular mass along the wall of the cystic mass protrudes inward. Some nodular enhancement is evident around the cystic mass lesion.
b: DWI of the same level as that of Fig. 5a. The high-intensity lesion of DWI corresponds approximately to the 3DFSPGR image.
c: ADC map of the same level as that of Fig. 5b. The low ADC area is absent.
d: The histopathologic figure neighboring the lesion of intracystic papillary carcinoma shows hemosiderine-laden macrophage surrounding the intraductal carcinoma component (black arrow; H&E, ×40).

cell density, tumor structure, intestinal structure, and tissue components such as edema, necrosis, and fibrosis. With regard to breast DWI, a high sensitivity to breast malignant tumor has been already proven. Y. Guo demonstrated 93% sensitivity with the threshold of 1.3×10^{-3} mm^2/s of ADC value for breast cancer, while Y. Kuroki et al. showed statistically lower ADC values for breast carcinomas than those of benign tumors.[3,15] Our study showed a 93% sensitivity to malignant tumors among the G-1, G-2, and G-3 cases, with a threshold of 1.6×10^{-3} mm^2/s of ADC value. As

for the false negative cases and underestimated cases, in which the ADC values were not decreased in the carcinoma components, notable histopathologic characteristics were observed in the specimens, specifically necrosis and hemorrhage. Seven cases of G-3 and 9 cases of G-4 showed hemorrhage or necrosis mainly owing to DCIS or malignant phyllodes tumor. Conversely, hemorrhage was also observed in some specimens of intraductal papilloma. However, most intraductal papilloma showed low ADC values. The reason for this anomaly is unknown. We speculate that the character of the hemorrhage differs between the malignant tumors and intraductal papilloma. Comedo-type DCIS show the phenomenon of necrosis, hemorrhage, and calcification. We hypothesize that the high degree of oxidation as a consequence of necrosis affects the high ADC value. Specifically, the strong effect of magnetic susceptibility is one mechanism of high ADC values in DCIS and malignant phyllodes tumor with bleeding. Since seven of the bleeding cases showed high intensity in T_1-weighted images, it is possible to speculate about the occurrence of hemorrhage by referring to other sequences.

In 3 cases categorized as G-3, scattering and sparse distribution of lobular carcinoma and DCIS did not represent low ADC values. Moreover, with respect to 11 cases categorized as G-1 in which the ADC map did not show low values in DCIS around main tumors, one reason for the misdiagnosis is the limited spatial resolution of DWI. However, the sensitivity to small foci and the sparse distribution of tumor will improve with advances in the spatial resolution of DWI.

As for benign lesions, although Guo et al. showed all fibroadenoma were correctly diagnosed as benign lesions, one case of duct ectasia and one of intraductal papilloma were incorrectly categorized.[3] In our study, specificity was markedly low. Most cases of intraductal papilloma and more than half the cases of fibrocystic disease showed low ADC values and were categorized as malignant lesions. Moreover, benign proliferative changes such as ductal hyperplasia, fibroadenosis, and lobular hyperplasia around the carcinoma have resulted in over-estimation of cancer extension. Some pathogenesis of this phenomenon can be considered. Guo et al. confirmed the relation between ADC values and cell density, which exhibited an inverse proportion. Fibrocystic disease sometimes shows a high cell density and inflammatory reactions. This phenomenon restricts proton diffusion, a possible reason for low ADC values. However, the disparity between the ADC values of fibrocystic disease and malignancy could be divided further with a higher b-value. This is because the effect of perfusion is smaller at higher b-values and the reduction in ADC values of malignant lesions is more prominent than that of benign lesions due to angiogenesis of malignant tumor.[16,30] Only two cases of fibroadenoma were found in our study, both of the pericanalicular type, and both exhibited low ADC values. Although Guo et al. did not mention the detailed type of fibroadenoma, it is possible that not all fibroadenoma will show high ADC values. Therefore, ADC values are still unreliable for fibrocystic disease, intraductal papilloma, and some types of fibroadenoma. As our study showed low specificity, DWI is still insufficient for qualitative diagnosis.

Conclusion

Our trial sought to verify the usefulness of breast DWI in clinical applications. We discovered that the sensitivity is sufficient for detecting malignant lesions. In addition, with DWI we were able to obtain images with one-minute scan times. This satisfies the requirements for screening use. This study demonstrated the potential for DWI to be used in the assessment of cancer extension. The spatial resolution and accuracy of differentiation will be improved with advances in MRI technology.

References

1. Filippi M, Cercignani M, Inglese M, et al. Diffusion tensor magnetic resonance imaging in multiple sclerosis. Neurology 2001; 56:304-311.
2. Bammer R. Basic principles of diffusion-weighted imaging. Eur J Radiol 2002; 45:169-184.
3. Guo Y, Cai YQ, Cai ZL, et al. Differentiation of clinically benign and malignant breast lesions using diffusion-weighted imaging. J Magn Reson Imaging 2002; 16:172-178.
4. Lyng H, Haraldseth O, Rofsrad EK. Mesurement of cell density and necrotic fraction in human melanoma xenografts by diffusion weighted magnetic resonance imaging. Magn Reson Med 2000; 43:828-836.
5. Warach S, Boska M, Welch KM. Pitfalls and potential of clinical diffusion-weighted MR imaging in acute stroke. Stroke 1997; 28:481-482.
6. Noguchi K, Watanabe N, Nagayoshi T, et al. Role of diffusion-weighted echo planar MRI in distinguishing between brain abscess and tumour: a preliminary report. Neuroradiology 1999; 41:171-174.
7. Tsuruda JS, Chew WM, Moseley ME, et al. Diffusion-weighted MR imaging of the brain: value of differentiating between extraaxial cysts and

epidermoid tumors. AJNR Am J Neuroradiol 1990; 11:925-931.
8. Kim T, Murakami T, Takahashi S, et al. Diffusion weighter single-shot echoplanar MR imaging for liver disease. AJR Am J Roentgenol 1999; 173: 393-398.
9. Namimoto T, Yamashita Y, Sumi S, et al. Focal liver masses: characterization with diffusion-weighted echo planar MR imaging. Radiology 1997; 04:739-744.
10. Kuroki S, Nasu S, Murakami K, et al. Pancreatic cancer on DWI. Nippon Acta Radiol 2003; 63: S184.
11. Moteki T, Ishizaka H, Horikoshi H, et al. Differentiation between hemangiomas and hepatocellular carcinomas with the apparent diffusion coefficient calculated from turboFLASH MR images. JMR 1995; 5:187-191.
12. Moteki T. Ishizaka H. Diffusion-weighted EPI of cystic ovarian lesions: evaluation of cystic contents using apparent diffusion coefficients. J Magn Reson Imaging 2000: 12:1014-1019.
13. Maier CF, Paran Y, Bendel P, et al. Quantitative diffusion imaging in implanted human breast tumors. Magn Reson Med 1997; 37:576-581.
14. Englander SA, Ulug AM, Brem R, et al. Diffusion imaging of human breast. NMR Biomed 1997; 10:348-352.
15. Kuroki Y, Katsushiro N, Kuroki S, et al. Diffusion-weighted imaging of breast cancer with the sensitivity encoding technique: analysis of apparent diffusion coefficient value. MRMS 2004; 3:79-85.
16. Buadu LD, Murakami J, Murayama S, et al. Breast lesions: correlation of contrast medium enhancement patterns on MR images with histopathologic findings and tumor angiogenesis. Radiology 1996; 200:639-649.
17. Mumtaz H, Hall-Craggs MA, Davidson T, et al. Staging of symptomatic primary breast cancer with MR imaging. AJR Am J Roentgenol 1997; 169: 417-424.
18. Morris EA, Schwartz LH, Dershaw DD, et al. MR imaging of the breast in patients with occult primary breast carcinoma. Radiology 1997; 205:437-440.
19. Boné B, Péntek Z, Perbeck L, et al. Diagnostic accuracy of mammography and contrast-enhanced MR imaging in 238 histologically verified breast lesions. Acta Radiol 1997; 38:489-496.
20. Stomper PC, Winston JS, Herman S, et al. Angiogenesis and dynamic MR imaging gadolinium enhancement of malignant and benign breast lesions. Breast Cancer Res Treat 1997; 45:39-46.
21. Boetes C, Barentsz JO, Mus RD, et al. MR characterization of suspicious breast lesions with a gadolinium-enhanced turbo FLASH subtraction technique. Radiology 1994; 193:777-781.
22. Heiberg EV, Perman WH, Herrmann VM, et al. Dynamic sequential 3D gadolinium-enhanced MRI of the whole breast. Magn Reson Imaging 1996; 14:337-348.
23. Baum F, Fischer U, Vosshenrich R, et al. Classification of hypervascularized lesions in CE MR imaging of the breast. Eur Radiol 2002; 12:1087-1092.
24. Fischer U, Kopka L, Grabbe E. Breast carcinoma: effect of preoperative contrast-enhanced MR imaging on the therapeutic approach. Radiology 1999; 13:881-888.
25. Orel SG, Schnall MD, Powell CM, et al. Staging of suspected breast cancer: effect of MR imaging and MR-guided biopsy. Radiology 1995; 196:115-122.
26. Rieber A, Merkle E, Böhm W, Brambs H-J, Tomczak R. MRI of histologically confirmed mammary carcinoma: clinical relevance of diagnostic procedures for detection of multifocal or contralateral secondary carcinoma. J Comput Assist Tomogr 1997; 21:773-779.
27. Boetes C. Strijk SP. Holland R. et al. False-negative MR imaging of malignant breast tumors. Eur Radiol 1997; 7:1231-1234.
28. Cohen EK, Leonhardt CM, Shumak RS, et al. Magnetic resonance imaging in potential postsurgical recurrence of breast cancer: pitfalls and limitations. Can Assoc Radiol J 1996; 47:171-176.
29. Liu PF. Debatin JF. Caduff RF, et al. Improved diagnostic accuracy in dynamic contrast enhanced MRI of the breast by combined quantitative and qualitative analysis. Br J Radiol 1998; 71:501-509.
30. Hulka CA, Smith BL, Sgroi DC, et al. Benign and malignant breast lesions: differentiation with echoplanar MR imaging. Radiology 1995; 197:33-38.

Diffusion-Weighted Imaging of Malignant Breast Tumors

The Usefulness of Apparent Diffusion Coefficient (ADC) Value and ADC Map for the Detection of Malignant Breast Tumors and Evaluation of Cancer Extension

Reiko Woodhams, MD, Keiji Matsunaga, MD,* Keiichi Iwabuchi, MD,† Shinichi Kan, MD,* Hirofumi Hata, RT,* Masaru Kuranami, MD,‡ Masahiko Watanabe, MD,‡ and Kazushige Hayakawa, MD**

Summary: The authors used breast diffusion-weighted imaging (DWI) to diagnose breast cancer and identify cancer extension. Isotropic DWI was performed with EPI. The apparent diffusion coefficient (ADC) value was calculated and displayed on an ADC map. The authors compared between the distribution of low ADC values and pathologic cancer extension. The mean ADC value of breast cancer was $1.12 \pm 0.24 \times 10^{-3}$ mm^2/s, which was lower than that of normal breast tissue. The ADC value for invasive ductal carcinoma was lower than that of noninvasive ductal carcinoma. The sensitivity of the ADC value for breast cancer using a threshold of less than 1.6×10^{-3} mm^2/s was 95%. Seventy-five percent of all cases showed precise distribution of low ADC value as cancer extension. The causes of underestimation were susceptibility artifact from bleeding and the limit of spatial resolution. Benign proliferative change showed a low ADC value. The authors conclude that DWI has a potential for clinical appreciation in detecting breast cancer.

Key Words: diffusion-weighted image, apparent diffusion coefficient map, malignant breast tumor, benign proliferative change, susceptibility artifact

(*J Comput Assist Tomogr* 2005;29:644–649)

Magnetic resonance imaging (MRI) is one of the diagnostic tools for breast evaluation. It has been assessed extensively as a valuable tool for breast diagnosis. MRI with enhancement provides high contrast resolution and results in high sensitivity for breast carcinoma. The utility for estimating the extension of breast carcinoma and evaluation for chemotherapy treatment is already recognized.[1–6] However, MRI has some disadvantages compared with mammography and ultrasound: it has a long scan time, the use of contrast is sometimes contraindicated because of allergy, and it is expensive. Sometimes it is difficult to differentiate a malignant lesion from a benign lesion by using a morphologic approach and enhancement pattern: benign hyperplastic change, metaplasia, and fibroadenoma sometimes show an enhancement pattern similar to that of malignancy.[7–9]

On the other hand, diffusion-weighted imaging (DWI) represents the biologic character of tissue. DWI reflects the random thermal motion of molecules (Brownian motion). Mainly the Brownian motion of protons in bulk water contributes to the signal in DWI. The apparent diffusion coefficient (ADC) is used to quantify the Brownian motion. In biologic tissue, ADC includes Brownian motion (incoherent motion) and capillary blood circulation (coherent motion). However, coherent motion is affected less with high diffusion-sensitizing factor (b-value). Decreased movement of molecules in the tissue correlates with a low ADC value.

DWI is already recognized as a first choice to diagnose brain infarction.[10] Recent improvements in hardware and imaging made with DWI have expanded its applications. Investigations have shown the possibility of using DWI on other organs to diagnose and differentiate (e.g., brain abscess, pancreas, and focal hepatic lesions).[11–14] The breast is no exception for the use of DWI adaptation. Englander et al initially studied the use of DWI for human breasts.[15] Guo et al showed the statistical difference of ADC value between malignancy and benign lesions and showed the high precision of ADC to differentiate breast tumors: sensitivity was 93% and specificity 88% with an ADC threshold of 1.30×10^{-3} mm^2/s.[16]

We analyzed the ADC value of normal mammary glands and malignant breast lesions to determine the threshold of the ADC value to distinguish between malignant lesions and normal lesions and examine the DWI sensitivity for the malignant lesions. We also compared the distribution of low ADC value on an ADC map with cancer extension of the pathologic specimen and evaluated the ability of the ADC map to analyze tumor extension. We also evaluated the pathologic phenomenon compared with an altered ADC value to research the factors affecting the ADC value.

Received for publication January 22, 2005; accepted May 18, 2005.
From the *Department of Radiology, Kitasato University School of Medicine, Kanagawa, Japan; †Department of Pathology, Kitasato University School of Medicine, Kanagawa, Japan; and ‡Department of Surgery, Kitasato University School of Medicine, Kanagawa, Japan.
Reprints: Reiko Woodhams, Kitasato University School of Medicine, 1-15-1, Kitasato, Sagamihara, Kanagawa, 228-8555, Japan (e-mail: reiko99@db3.so-net.ne.jp).

METHODS

Subjects

Seventy-six patients with breast carcinoma underwent MRI, including DWI scans. All patients were female; their age ranged from 30 to 80 years (mean 53). Tissue samples were available from each patient: 31 patients underwent Auchincloss surgery and 45 had breast-conserving surgery.

Histopathologic Data

All tissues were fixed in 10% formalin and embedded in paraffin. Four-micron-thick paraffin sections were cut every 3 to 10 mm from the excised tissues. The excised materials were sliced vertically to the lines from the tumors to the nipple side. The specimens were stained with hematoxylin and eosin. The average number of the slides per case was 13 (range 5–32). All of the specimens underwent microscopic examination. There were 66 invasive ductal carcinomas (IDCs) and 10 noninvasive ductal carcinomas (NIDCs) (Table 1). The mean size of the malignant lesions was 22 mm in diameter (range 7–70 mm).

MRI Protocol

MRI was performed on a GE Signa CV/i 1.5T Version 9.1 by using a breast coil (surface coil). Prior to DWI, FRFSE using CHESS for fat saturation in the sagittal plain was performed. After DWI in the axial plane, 3D FSPGR using Spec IR for fat saturation in the sagittal plane before and after administration of gadopentetate dimeglumine (0.2 mmol/kg) was obtained. Subtraction images were produced with 3D FSPGR for identification of enhancement. 2D FSPGR with CHESS in the axial plane was obtained after enhancement. Imaging parameters were as follows: 2D FRFSE (TR = 3,000, eff TE = 85, 256 × 192, 3 NEX), DWI [spin-echo single-shot echo planar image (EPI), motion probing gradient (MPG) were applied along the *x*, *y*, and *z* axes (isotopic DWI) before and after the 180-degree pulses to obtain the images used for synthesizing isotropic images, b-value 0 and 750 s/mm^2, TR/TE: 5,000/61.8, image matrix: 128 × 128, field of view: 320 mm × 240 mm, slice thickness: 6 mm, spacing: 1 mm, 5 NEX, acquisition time: 60 s], 3D FSPGR (TR = 5.7, TE = 1.2, flip angle 20 degrees, image matrix: 256 × 160, 2 NEX), 2D FSPGR (TR = 200, TE minimum, flip angle 90 degrees, image matrix: 512 × 192, 3 NEX).

TABLE 1. ADCs According to Histopathology

	n	Mean ADC Value ($\times 10^{-3}$ mm^2/sec)
DCIS	9	1.31 ± 0.57
Solid tubular Ca	23	1.13 ± 0.55
Lobular Ca	8	1.07 ± 0.56
Scirrhous Ca	17	1.07 ± 0.54
Papillotubular Ca	15	1.05 ± 0.52
Intracystic papillary Ca	1	2.5
Medullary Ca	1	1.2
SCC	1	1.1
Adenoid cystic Ca	1	1.0
Total	76	

ADC, apparent diffusion coefficient; SCC, squamous cell carcinoma.

Analysis of ADC Values

ADC values were calculated according to the formula ADC = −(1/b)In(S/So), where So and S were the signal intensities in the region of interest (ROI), obtained with two different gradient factors (b value of 0 and 750 s/mm^2). ADC distribution was demonstrated on an ADC color map using Advantage Workstation Version 4.0 (GE). ROIs were placed in the area of malignant lesions and normal mammary gland lesions on ADC map by referring to subtraction images originating from 3D FSPGR and 2D FSPGR in the axial plane after enhancement. The sizes of the ROIs were 5 to 10 mm in diameter, depending on the size of the tumors. The ROIs of malignant lesions had to be smaller than the mass size, not including normal tissue. Two diagnostic radiologists chose the areas that showed the strongest enhancement visually, and ADC values were averaged. The size of the ROI in normal tissue was 10 mm in diameter. Each ROI was placed twice by one diagnostic radiologist, and ADC values were averaged. In addition, the ADC values between NIDC and IDC were compared. Predominant NIDC was included in the NIDC category. The threshold of the ADC value for a malignant lesion was determined as a low ADC value by the results from above.

Comparison Between ADC Map and Specimens

A radiologist retrospectively identified the area of interest on the ADC map. This was pathologically examined, and a radiologist and a pathologist investigated the relationship between the ADC map and the pathologic figures. To determine the orientation of the tumors and the breast areas on the specimens, we referred to the relationship between nipple marking and main tumor position on the excised material from surgery.

The area of low ADC values were depicted on the ADC map with a certain color and compared with tumor distribution on the specimen. The areas that were not surgically excised and not pathologically evaluated were not included in this investigation. We categorized the correlation between the ADC map and tumor extension in four groups (Table 2). In group 1, the area of low ADC value was almost the same as tumor spread. In group 2, the overdiagnosed group, the area of low ADC value was wider and more than twice the area of tumor spread. In group 3, the underdiagnosed group, the area of low ADC value was smaller and less than half of the area of tumor spread. Group 4 was the false-negative group.

Statistics

The Wilcoxon signed rank sum test was used for analyzing differences of mean ADC values for significance

TABLE 2. Classification of Groups

Group No.	Group Description	n	
1	Precise group	57	75%
2	Overdiagnosed group	15	20%
3	Underestimated group	3	4%
4	False-negative group	1	1%
	Total	76	

between breast cancer and normal breast tissue and between IDC and NIDC or predominant NIDC. The honestly significant difference (HSD) of Tukey-Kramer was used to compare the mean ADC value between solid tubular carcinoma, lobular carcinoma, scirrhous carcinoma, and papillotubular carcinoma.

RESULTS

Measurement of ADC Values

The mean ADC value of normal breast tissue was $2.05 \pm 0.27 \times 10^{-3}$ mm²/s; that of malignant lesions was $1.12 \pm 0.24 \times 10^{-3}$ mm²/s (Fig. 1). The difference between them was significant ($P = 0.001$). According to this result, the threshold of low ADC values for a malignant lesion was determined to be less than 1.6×10^{-3} mm²/s. The mean ADC value for IDC was $1.09 \pm 0.23 \times 10^{-3}$ mm²/s; that for NIDC was $1.42 \pm 0.42 \times 10^{-3}$ mm²/s. The difference between them was significant ($P = 0.0004$) (Fig. 2). The mean ADC value for each pathologic type is shown in Table 1. Among the four major types of IDC, there was no significant difference in the ADC value.

Comparison Between ADC Map and Tumor Spread

Fifty-seven cases (75% of all cases) were in group 1. The area of low ADC value corresponded with the tumor distributions. Fourteen cases (16%) were in group 2, overdiagnosis of tumor extension (see Table 2). In nine cases in group 2, histology-proven fibrocystic change, apocrine metaplasia, and ductal or lobular hyperplastic area showed a low ADC value and did not include a carcinoma component (Fig. 3). These

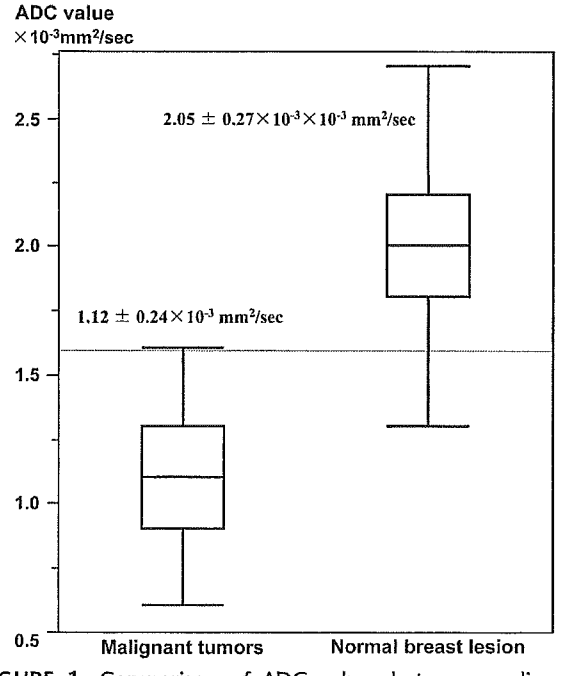

FIGURE 1. Comparison of ADC values between malignant lesions and normal lesions.

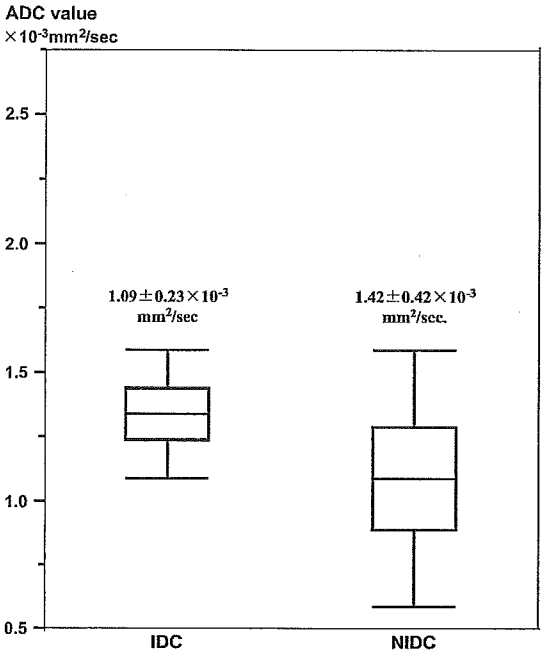

FIGURE 2. Correlation of ADC values between IDC and NIDC. IDC values were lower than NIDC values.

cases showed segmental and spotty distribution of low ADC value around the primary malignant lesion. The mean ADC value of these proliferative changes was 1.34×10^{-3} mm²/s (range $1.1–1.5 \times 10^{-3}$ mm²/s).

Three cases were in group 3 and one case was in group 4 (Table 3). Two cases in group 3 were invasive lobular carcinoma. The ADC map in these cases showed a low ADC area on the solid core of the tumor. However, the ADC map did not depict the sparse distribution and small foci of lobular carcinoma widely spread in the mammary gland and fat tissue (Fig. 4). One case in group 3 and the one case in group 4 showed comedo-type ductal carcinoma in situ (DCIS), which contained remarkable hemorrhage and necrosis. Also, hemosiderin deposition around ducts was observed in the pathologic figure of the group 4 case (Fig. 5).

DISCUSSION

DWI has a new potential in the approach to the biologic and structural character of tissues. Previous reports suggested that a low ADC value might indicate high cell density, dense mucus tissue, and fibrosis.[11–13,16,17–19] Although the mechanism of DWI appearance is still uncertain, the use of DWI for diagnosis and differentiation of diseases has been recently spreading from the central nerve system to other organs.[10–14,16,17,20] This advance is due largely to the EPI sequence, which shortens the scan time and minimizes motion artifact.[21] Our results in the present study showed 95% sensitivity for malignant tumors by DWI with only a 1-minute scan time, which is equivalent to the findings of Guo et al[16] and Kuroki et al.[20] DWI showed high sensitivity for breast cancer and a short scan time.